Synthesis and biological evaluation of novel tetranuclear cyclopalladated complex bearing thiosemicarbazone scaffold ligand: Interactions with double-strand DNA, coronavirus, and molecular modeling studies

Zohreh Mehri Lighvan, Hossein Ali Khonakdar, Ali Akbari, Maryam Dehdashti Jahromi, Azar Ramezanpour, Anthony Kermagoret, Abolfazl Heydari, Esmaiel Jabbari

Synthesis and biological evaluation of novel tetranuclear cyclopalladated complex bearing thiosemicarbazone scaffold ligand: Interactions with double-strand DNA, coronavirus, and molecular modeling studies

Zohreh Mehri Lighvan[1] | Hossein Ali Khonakdar[1,2] | Ali Akbari[3] | Maryam Dehdashti Jahromi[4] | Azar Ramezanpour[5] | Anthony Kermagoret[6] | Abolfazl Heydari[7] | Esmaiel Jabbari[8]

[1]Department of Polymer Processing, Iran Polymer and Petrochemical Institute, Tehran, Iran
[2]Leibniz-Institut für Polymerforschung, Dresdene. V, Dresden, Germany
[3]Solid Tumor Research Center, Cellular, and Molecular Medicine Research Institute, Urmia University of Medical Sciences, Urmia, Iran
[4]Faculty of Engineering, Jahrom University, Jahrom, Iran
[5]Department of Chemistry, Isfahan University of Technology, Isfahan, Iran
[6]Aix Marseille Univ, CNRS, ICR,Marseille, France
[7]Polymer Institute of the Slovak Academy of Sciences, Bratislava, Slovakia
[8]Department of Chemical Engineering, University of South Carolina, Columbia, South Carolina, USA

Correspondence
Zohreh Mehri Lighvan, Department of Polymer Processing, Iran Polymer and Petrochemical Institute, P.O. Box 14965-115, Tehran, Iran. Email: z.mehri@ippi.ac.ir
Ali Akbari, Solid Tumor Research Center, Cellular and Molecular Medicine Research Institute, Urmia University of Medical Sciences, Shafa St, Ershad Blvd., P.O. Box 5715789400, Urmia, Iran. Email: akbari.a@umsu.ac.ir

Funding information Iran National Science Foundation, Grant/Award Number: 97006605

Abstract

Threading intercalators are a novel class of materials that carry two substituents along the diagonal positions of an aromatic ring. When bound to DNA, these substituents project out in DNA grooves. Tetranuclear complexes appear to be promising threading intercalators for developing therapeutics against cancer and viral infections that require high nucleic acid binding affinity. The objective of this work was to prepare the thiosemicarbazone scaffold ligand [4-$ClC_6H_4CHN{=}NC(S)NHPh$] and tetranuclear cyclopalladated complex [$Pd(4\text{-}ClC_6H_4CHN{=}NC(S)NHPh)_4$] and to characterize the compounds by elemental analysis, 1D and 2D NMR, HRMS, and IR spectroscopy. The calf thymus DNA (CT-DNA) binding properties of the compounds were investigated in vitro under simulated physiological conditions using UV–vis spectroscopy, emission spectral titration, methylene blue competitive binding, circular dichroism, DNA thermal denaturation, DNA binding, and coronavirus interactions using molecular simulation. The compounds showed cytotoxic effect against both human breast (MCF-7) and colorectal (HCT116) cancer cells in a dose-dependent manner. We demonstrated that the compounds are promising for DNA threading intercalation binders with large DNA binding constants on the order of 10^7 M^{-1} magnitude.

KEYWORDS
anticancer, cyclopalladated, DNA, thiosemicarbazones scaffold, threading intercalation

1 | INTRODUCTION

The prevalence of cancer and parasitic diseases has posed a huge health risk to people in developing countries with a narrow spectrum of effective drugs available for treatment. Organometallic compounds display a range of characteristics providing pharmacological profiles which are not attainable by organic molecules.[1] In fact, many organometallic compounds have been designed to specifically bind to a well-defined target site on biomolecules.[2,3] In the bioinorganic systems, cyclopalladated
complexes, due to their high lability in biological fluids, are promising antitumor drugs that are effective in both in vitro and in vivo environments, when compared with platinum group metal (PGM) as an anticancer compounds.[4,5] The cyclopalladated complexes are more stable and significantly less toxic, suggesting they could
possess a more specific in vivo antitumor activity.[6–8] In particular, orthometallated N-donor ligands, such as thiosemicarbazones, benzylamines, and imines, have been successfully used as targeted antitumor drugs due to
the presence of a strong palladium-carbon σ-bond in the "(C,N)Pd" metallacycle, which enhances the stability of the organometallic complex.[9] Some reports have shown that cyclopalladated compounds interact with thiol groups of mitochondrial membranes to induce apoptotic cell death via the intrinsic pathway.[10,11] The other reports show that the antitumor activity of cyclopalladated compounds is dependent on their interaction with DNA.[12,13] The antitumor activity of cyclopalladated compounds is believed to be due to the inhibition of DNA synthesis resulting from changes in reaction conditions in reductive conversion of ribonucleotides to deoxyribonucleotides.[14] Thiosemicarbazones (TSCs) scaffold as ligands are an important class of bioactive compounds with a wide range of properties ranging from their use as anticancer agents[15] to antiviral,[16] antibacterial,[17] antiproliferative,[18] anti-leprosy,[19] antimalarial,[20] antitubercular,[21] and antiparasitic[22–24] agents. The anticancer activity of thiosemicarbazones stems from their chelating ability with transition metal ions by bonding
through the sulfur and the azomethinic nitrogen atoms to inhibit the biosynthesis of DNA, possibly by blocking the enzyme ribonucleotide diphosphate reductase.[25,26] Notably, chelating ligands have been used to overcome this
high lability, forming thermodynamically stable and kinetically inert cyclopalladated complexes.[27,28] Demertzi et al. reported Pd(II) complexes of N4-alkyl-2-acetylpyridine thiosemicarbazones inhibits the activity of DNA synthesized in L1210 and P388 cell cultures.[29] In a study by Quiroga et al., Pd(II) and Pt(II) complexes of phenylacetaldehyde thiosemicarbazone and binuclear chloro-bridged palladated and platinated complexes derived from p-isopropylbenzaldehyde

thiosemicarbazone
showed activity against several human and murine cell lines (HL-60, U937, HeLa, and 3T3) that are resistant to the clinically used cisplatin.[30,31]
DNA plays a crucial role in a wide variety of cellular processes[32] and serves as a superior target for the treatment of treating genetic diseases like cancer.[33] The anticancer, antiparasitic, and antimicrobial agents exert their biological response via interaction with ellipticine, which unwinds DNA and inhibits the processes of transcription, replication, and DNA repair mechanisms.[34]
The COVID-19 epidemic has caused in a global health emergency and has spread to 213 countries and is uncontrollable so far.[35] CoVs (COVID-19) are positive-stranded RNA viruses with a crown-like appearance under an electron microscope due to the presence of spike glycoproteins on the envelope. Two groups of proteins characterize CoVs. The first group is structural proteins such as Spike (S) that are common in all coronaviruses, that is, Nucleocapsid (N), Matrix (M), and Envelope (E). The second group is the nonstructural proteins, such as proteases (nsp3 and nsp5) and RdRp (nsp12).[36,37] The Spike protein is a crucial recognition factor for virus attachment and entry to the host cells. It is present on the virion's outer surface in a homo-trimeric state.[36] The RNAdependent RNA polymerase (RdRp, also named nsp12)
is the central component of coronaviral replication/ transcription machinery and appears to be a primary target for the antiviral drug, remdesivir.[38] It has been reported that TSCs possess antiviral as well as antiHIV properties.[39,40] A series of isatin-β-thiosemicarbazones have been tested against herpes simplex virus type 1 (HSV-1) and type 2 (HSV-2).[41] Hence, we hypothesized that the synthesis and testing of more novel TSC compounds could be beneficial to understanding the mechanism of their antiviral activity.
As part of our ongoing research and interest in the structural chemistry of palladium compounds,[42–47] we have turned our attention to cyclopalladated thiosemicarbazone complexes. Herein, we report on the synthesis, structural characterization, DNA interaction, and cytotoxicity of cyclopalladated thiosemicarbazone. The molecular docking technique is used to determine the mechanism of interaction of the complex with DNA and RNA.

2 | RESULTS AND DISCUSSION

2.1 | Synthesis and characterization of the compounds

The synthesis process and the chemical structure of the thiosemicarbazone ligand (TSC) and cyclopalladated thiosemicarbazone (Pd-TSC) used in this study are shown in Scheme 1. The chemical structure of the compounds was characterized by elemental analysis (C, H, N, and S), IR spectroscopy, and 1D including ^{1}H and ^{13}C NMR modes and 2D NMR, including COSY and HMQC modes.

The infrared (IR) spectra of compounds were performed for identifying the functional groups of the ligand and the complex (see Supporting Information). The IR spectrum of the ligand shows bands at 3309 and 3138 cm^{1}, which are attributed to N–H and N–H $_{hydrazinic}$ stretching vibrations, respectively, and bands in the ranges 1597–1536 cm^{1} and 815–743 cm^{1} are corresponding to C=N and C=S stretching vibrations, respectively. This is in agreement with the reported values.[48] Comparison of the spectra of the complex with the free ligand shows the disappearance of N–$H_{hydrazinic}$ and C=S bands, as identified by others.[49] The C=N band has shifted to lower wavenumbers upon complex formation by approximately 40 cm^{1} in agreement with coordination of the palladium atom to the C=N moiety through the lone nitrogen pair.[50,51] Additionally, the presence of a new band at 687 cm^{1} in complex, attributed to C–S stretching vibration, indicated coordination of Pd via the sulfur atom in the thiol form.[14] The electronic spectra of the complexes showed the intra-ligand bands in the 230–266 nm and 350–372 nm ranges, corresponding to the n ! π* and π ! π* transitions, respectively.

The chemical structure of thiosemicarbazone ligand (TSC) and cyclopalladated thiosemicarbazone complex (Pd-TSC) were characterized by the ^{1}H NMR, ^{13}C NMR, COSY, and HMBC spectra in DMSO-d_6. Figure 1a shows ^{1}H NMR spectra of the TSC ligand that is exhibited the secondary = N–H– and –NHPh– proton signals at 10.16 ppm and 11.86 ppm, respectively. In addition, a singlet associated with the –CH=N– (H6) proton observed at 8.15 ppm and the signals in the range of 7.20–7.96 ppm were attributed to aromatic protons (Figure 1a) with the help of COSY experiments. No signal at around 4.00 ppm (i.e., the –SH proton) was observed in the ^{1}H NMR spectra of the TSC, indicating that it remained solely in the thione form, even in a polar solvent like DMSO-d_6, as reported by others.[52] APT ^{13}C NMR and 2D HMQC experiment confirmed the ligand structure and permitted to identify the S=C signal at 176.7 ppm, the imine (–N=CH6–) signal at 141.9 ppm and the eight aromatic signals between 140 and 124 ppm (see Supporting Information).

The reaction of potassium tetrachloropalladate and 1.1 equiv. of TSC ligand afforded the Pd-TSC complex in good yield. In contrast to the ^{1}H NMR spectrum of TSC (Figure 1a), the proton signal of NH imine group was not observed upon formation of the complex, demonstrating the deprotonation of =N–NH group, thus

confirming metalation.[49] The two singlets at 9.61 and 9.34 ppm were assigned to the NH function, where the H is possibly in equilibrium between the two nitrogen atoms of the thiosemicarbazone group (see Supporting Information).

To the best of our knowledge, this equilibrium was not reported in the literature, but RX-crystal structures presented a =N–NH–C(S)=N– metallocycle structures[52,53] or a =N–N=C(S)–NH–.[14,48,54–56] This possible equilibrium would affect the proton aromatic signals, leading of a two set of signals for protons H1–$H1_0$, H2–$H2_0$, and H3–$H3_0$ but difficultly identified in the complicated aromatic region (8.4–6.8 ppm) of the Pd-TSC ^{1}H spectrum. The COSY NMR experiment permitted to suggest the present proton signal assignation (see Supporting Information) but several signals remained unassigned. Normally, the ortho and para protons, with respect to the palladium atom, are more affected by the metalation.[14] APT ^{13}C NMR of Pd-TSC permitted to observe five C_{IV} signals, in good agreement to the proposed structure of the cyclopalladated complex. The ^{13}C-APT signals of the C=S carbons of the ligand (176.6 ppm) shifted upfield to 168.1 ppm for tetrameric compound, indicating coordination of Pd with S and N and attached to ortho C of phenyl ring (Figure 1). However, the ^{13}C aromatic region (135–115 ppm) was not well defined. The HMBC NMR experiment allowed to correlate the proposed ^{1}H NMR signals and the ^{13}C signals. More interestingly, ^{1}H signals at 9.61 and 9.34 ppm were nor corelated to ^{13}C signal, confirming their assignation to the NH group.

While the NMR spectra of Pd-TSC clearly showed a strong chemical modification compared with the ligand NMR spectra and elemental analysis are in good agreement with the proposed complex, the structure of cyclopalladated thiosemicarbazone complex was ascertained by high resolution mass spectrometry. Using the negative electrospray technique, the isotopic pattern measured at m/z 1574.715 for [$C_{56}H_{39}N_{12}S_4Cl_4Pd_4$] was identified and confirmed the tetranuclear character of the cyclopalladated thiosemicarbazone complex (see Supporting Information).

2.2 | Nucleic acid binding

Understanding the non-covalent binding of transition metal complexes to nucleic acids are an important aspect for developing new therapeutic agents and molecular probes. Many anticancer and antiviral compounds exert their therapeutic effect through intercalation with the nucleic acids of DNA, thereby interfering with DNA. This is the basis of designing novel anticancer therapeutics with greater efficiency, where effectiveness depends on mode and affinity of DNA binding.

2.3 | Study of DNA-tetranuclear complex interaction with UV–vis spectroscopy

A novel method for characterizing the type of DNA interaction with organometallic complexes is electronic absorption spectroscopy.[33] The absorption spectra of the thiosemicarbazones scaffold ligand and its Pd(II) complex in the absence and presence of CT-DNA are shown in Figure 2. Electronic absorption of the ligand showed two bands at 376 and 324 nm that were assigned to n-π* transition and one band at 248 nm that

was assigned to π-π* transition. Following the addition of CTDNA to the ligand solution, 28.05, 35.27, and 31.18% hypochromism was observed at 376, 324, and 226 nm, respectively. Further, the absorption band at 324 nm exhibited approximately 2-nm red shift due to a change of polarity in the ligand's microenvironment.[57] It is well known that the "hyperchromic effect" results from the damage to the structure DNA double helix, which leads to DNA contraction in the direction of helix axis and changes to DNA conformation.[58] Such marked hypochromic effect in spectrum of ligand confirmed the significant interaction of ligand with DNA. Typically, the hypochromic effect occurs via noncovalent interaction including intercalation and groove binding modes.[59]

The spectrum of Pd(II) complex exhibited absorption bands at 228, 256, and 350 nm with 26.53, 27.48, and 6.65% hypochromism, respectively. The absorption intensity of the complex decreased after the addition of DNA, due to noncovalent binding (hypochromism), as shown in Figure 1b.

The exact mode of binding can be determined by calculating the intrinsic binding constant (K_b) between the ligand and Pd(II) complex using Equation 1.[60]

$$\frac{[DNA]}{(\varepsilon_a - \varepsilon_f)} = \frac{[DNA]}{(\varepsilon_b - \varepsilon_f)} + \frac{1}{k_b(\varepsilon_b - \varepsilon_f)} \quad (1)$$

where ε_a, ε_b, and ε_f are extinction coefficients for the apparent, bound, and free compound, respectively. The coefficient ε_f was calculated from the standard curve of the isolated compound in a buffer solution using Beer's law. The coefficient ε_a was calculated as the ratio of the observed absorbance (A_{obs}) over the concentration of the complex, that is, A_{obs}/[complex]. A plot of [DNA]/(ε_a ε_f) versus [DNA] gives a slope of 1/(ε_b ε_f) and a y-intercept of 1/K_b (ε_b ε_f); therefore, K_b is determined from the ratio of the slope to the y-intercept (see inset of Figure 2). Using the above approach, the K_b values of 1.50 10^7 and 2.68 10^7 M^{-1} were obtained for the ligand and Pd(II) complex, respectively. One approach to increase DNA binding affinity to tetranuclear complexes is to reposition the active ligand for coordination with the metal.[61,62] Therefore, we used thiosemicarbazone as a ligand to improve anticancer and antiviral potential of tetranuclear complexes. Based on our calculations, the larger value of K_b indicates higher affinity for DNA binding to the Pd(II) complex as compared with the ligand alone. The Pd(II) complex contains four ligands for stronger DNA interaction. The K_b value of the complex is comparable with those complexes that interact with DNA via threading intercalation.[63,64] Therefore, it can be concluded that Pd(II) complex binds to different DNA sites on the basis of the structure. As the DNA double helix possesses many hydrogen binding sites that are accessible both in the minor and major grooves, it is likely that the –NH– group, N and Cl atoms of the Pd(II) complex formed hydrogen bonds with DNA, which led to the observed hypochromism in the absorption spectra of the Pd(II) complex. Conversely, our Pd(II) complex possesses aromatic rings that bind to DNA base pairs by intercalation. This type of Pd(II) complex binding engages more DNA bases, which, in turn, causes inhibition of replication and inefficient transcription. When synthesizing DNA-targeted drugs, high DNA binding affinity and slow DNA binding kinetics are considered important factor to

enhance therapeutic effects.[65,66] These desired properties are found in compounds that interact with DNA by threading intercalation, an interaction that first requires non intercalating moieties of a ligand to pass between DNA base pairs prior to intercalative binding.[67,68] High binding affinity is related to the stability of Pd complex. The tetranuclear nature and stable Pd–S bonds contribute to the stability of Pd(II) complex even in the presence of nucleophiles like DNA bases.[53] Considering high mortality of patients inflicted with cancer and viral infection, particularly those infections transmitted via the respiratory route, we hypothesized that the thiosemicarbazones scaffold ligand and its tetranuclear cyclopalladated complex could potentially serve as an efficient carrier for cancer therapeutics and antiviral agents targeting DNA and RNA.

2.4 | Competitive displacement assay with MB

The competitive interaction assay of ligand and Pd(II) complex was performed with DNA bound Methylene Blue (MB) to determine the interaction mode of DNA with the ligand and Pd(II) complex. Figure 3 shows the emission spectra of DNA bound MB in the presence of different concentrations of the ligand and Pd complex with excitation wavelength of 630 nm. The emission intensity of MB slowly increased following the addition of ligand. This result indicated that the ligand inserts itself in the DNA double helix, which is a characteristic of intercalative mode of binding. Consequently, the addition of Pd(II) complex has resulted in a more efficient change in emission intensity. Therefore, it could be concluded that the ligand and Pd(II) complex interacted with DNA mainly by intercalative mode.[69,70]

2.5 | Electronic circular dichroism

Electronic circular dichroism (ECD) is used extensively in the characterization of helical structure of DNA and its A, B, and Z-forms as well as their complexes with ligands.[71] The ECD spectrum of right handed B-DNA exhibits a positive band at 220 nm due to hydrogen bonding, a negative band at 240 nm due to handedness/polynucleotide helicity,[72] and a positive band at 275 nm due to base stacking.[73] Figure 4 depicts the ECD spectra of DNA in the presence of the ligand and Pd(II) complex are compared with that of DNA in the presence of Actinomycin D (ActD), as a threading intercalator.[74] When DNA was incubated with the Pd(II) complex at a molar ratio of 0.5, [complex]/[CT-DNA], the complex broadly induced spectral changes similar to that of DNA-ActD. Specifically, the complex and ActD binding to DNA induced a significant increase in the intensity of negative CD band at 240 nm along with a 4-nm red shift. The change in band intensity and a shift in wavelength at 240 nm can be attributed to a change in base pair geometry and a reduction in stacking interaction between the DNA bases as a result of the complex or ActD intercalation with the DNA base pairs.[75] The band attributed to right-handed helicity at 275 nm showed a large increase in intensity along with a slight red shift of 2 nm. These changes indicate alteration in duplex helicity of the DNA by interaction with the complex or ActD in which it forms a reversible, non-covalent and stable complex with DNA.[76] These observations support the threading intercalative mode of interaction

between the DNA and the Pd-ligand complexes.[77,78] In addition to threading intercalation binding mode, the CD spectral changes induced by Pd-ligand complexes and ActD reveal groove binding intercalation mode that stabilizes the right handed B-DNA, indicating and that the DNA unwounds upon interaction with the compounds.[75] These results are in conformance with our UV–vis studies which show distortion in the B-DNA conformation upon binding with the compounds.

2.6 | Hyperchromic effect of melting DNA with the compounds

DNA melting refers to the separation of double strands of DNA upon heating due to the breaking of hydrogen bonds between the DNA bases, which is greatly affected by the presence of other binding molecules.[79] The intercalation leads to a considerable increase in DNA melting temperature (T_m), as measured by the temperature at which the hypochromicity at 260 nm is reduced by half,[80] due to the stabilization of DNA duplex, whereas groove binding or electrostatic interactions leads a smaller change in the value of T_m.[44,81]

The melting curves of DNA in the absence and presence of compounds 1, 2, and ActD are shown in Figure 5. In the absence of compounds 1–3, the T_m of DNA was 83.01C. However, in the presence of compounds 1, 2, and 3, the T_m of DNA increased from 83.01C to 87.67, 88.86, and 88.08C, respectively, corresponding to ΔT_m values of 4.66, 5.85, and 5.07C.

The ΔT_m values in the presence of compounds 1–3 were slightly lower than 7.1C for threading intercalating of Act-D.[80] In fact, ethidium bromide (EB) causes significantly higher change of 13C in the melting temperature of DNA even at a relatively low [EB]/[DNA] ratio of 0.10.[82] We can infer from the DNA T_m results that compounds 1 and 2 bind by threading intercalation to DNA, leading to increased stability of the DNA double helix.[80,83]

2.7 | Molecular docking with DNA and human coronavirus Mers and coronavirus disease 2019

Molecular docking is a computational procedure and aims to predict the favored orientation of a ligand to its macromolecular target (receptor), when these are bound to each other to form a stable complex.[84] After the development of the first algorithms, molecular docking has become an important common and suitable computational tool of the drug discovery toolbox.

As it has relative low-cost implications and perceived simplicity of use, the molecular docking techniques became essential tool in drug discovery.[85] Also the interaction of any complex with the target biomolecule can be predict via molecular docking. The interaction between a complex and the biomolecules plays important role in many biological processes. In this study, the molecular docking calculations were used to investigate the interaction of the simple ligand structure and the complex structure with DNA and human coronavirus Mers and coronavirus disease 2019.

The optimized structure of the ligand and the complex is demonstrated at Figures 6 and 7, respectively.

Semiempirical methods employing PM6 functional was used for the optimization. The structure of the ligand

+ DNA and the interactions of ligand atoms and DNA residues are depicted in Figure 8a,b, respectively, while the structure of complex + DNA system and the interactions of complex atoms and DNA residues are depicted in Figure 9a,b, respectively. According to the calculation, the interaction between the ligand and DNA seems to be intercalation while the interaction of the complex and DNA seems to be almost threading intercalation. The calculated free binding energy of the interaction of the complex with DNA is 8.71 kcal/mol, and the calculated free binding energy of the interaction of the ligand with DNA is 6.86 kcal/mol. The structure of ligand + human coronavirus Mers system and the interactions between the ligand atoms and the binding sites of receptor are shown in Figure 10 while the structure of the complex + human coronavirus Mers system and the interactions between the complex atoms and the binding sites of receptor are shown in Figure 11. As shown in the Figures 10b and 11b, the 10 residues are involved in the interaction of the ligand with human coronavirus Mers as the same as the complex with human coronavirus Mers. The calculated free binding energy of the interaction of the complex with the receptor is 5.03 kcal/mol, and for the ligand + receptor system, the calculated free binding energy of the interaction is 5.29 kcal/mol. Figures 12a,b and 13a,b demonstrate the ligand + coronavirus disease 2019 and the complex + coronavirus disease 2019 systems and the interactions between the ligand and complex atoms and the binding sites of the receptor, respectively. The calculated free binding energies of the interaction of the complex with the receptor and the ligand with the named receptor are 10.11 and 8.32 kcal/mol. As the docking calculations show, the involved residues of the receptors in the interaction with the host molecules are clearly more in the receptor + complex structure system (18 residues) than in the ligand + receptor system (11 residues).

2.8 | In vitro cytotoxicity using MTT assay

The cytotoxicity of the synthesized ligand and complex was assessed against human MCF-7 breast cancer cells and HCT116 colorectal carcinoma cells for 24, 48, and 72 h with MTT assay. Cisplatin was used as a control group. The complex showed cytotoxic effect against both cell lines and the effect were concentration dependent (Figure 14a,b). The viability of MCF-7 and HCT116 cells decreased with increasing concentration of either the complex or the ligand. In the 0.05- to 0.4-mM concentration range, the ligand toxicity against HCT116 and MCF-7 cells was 24.07%–83.26% and 1.0%–80.0% after 24 h incubation, respectively. The complex in the same concentration range showed the values of 28.9%–94.2% and 5.39%–90.23%. The ligand showed a slightly higher cytotoxicity against both MCF-7 and HCT116 cells compared with the complex, while the difference was not significant. The cytotoxicity results demonstrate that the coordination of ligand to Pd has no significant effect on cytotoxicity of the complex against both HCT116 and MCF-7 cells. Moreover, the ligand and the complex exhibited low and high toxicity,

respectively, on HCT116 and MCF-7 cells compared with cisplatin.

3 | CONCLUSION

This work describes the synthesis, tumor toxicity, and antiviral activity of thiosemicarbazone scaffold ligands and their binding to the tetranuclear cyclopalladate complex. The structures of the synthesized compounds were elucidated spectroscopically and by diffractometry. Methylene blue displacement experiments showed support for an intercalative binding mode between DNA and the compounds. The DNA binding experiments using electronic spectral technique showed evidence for the hypochromic effect and small red shift with a DNA binding constant on the order of 10^7 M_1, consistent with intercalation and groove binding modes. According to CD spectrometry results, the compounds stabilized stabilization of the right-handed B form of DNA and, to a lesser extent, the DNA double strand. A ΔT_m value of 4.5–5.5C in the presence of the compounds was evidence for a mixed binding mode of interaction with the threading mode as the dominant mode, which was verified by docking simulations. The complex and the ligand showed cytotoxic effect against both human breast (MCF-7) and colorectal (HCT116) cancer cells and the effect was concentration dependent. The results demonstrate that the palladacycle complex [Pd(4-ClC6H4CHN=NC(S)NHPh)$_4$] has higher potency than the standard cisplatin chemotherapeutic.

4 | EXPERIMENTAL SECTION

4.1 | General material and methods

These are given in the Supporting Information.

4.2 | Synthesis of ligand (compound 1)

A 140-mg 4-chlorobenzaldehyde (1 mmol) in 30-ml MeOH was added to a suspension of 167-mg Nphenylhydrazinecarbothioamide (1 mmol) in 20-ml MeOH, in a round bottom flask. The reaction was proceeded under stirring at ambient temperature for 18 h. After completion of the reaction, the white precipitate was filtered, washed with cold MeOH, and dried under ambient condition. The resulting ligand was isolated and characterized as follows: Yellow solid (63.4%); mp: 207–208C (dec.). Anal. calc. for $C_{14}H_{12}ClN_3S$: C, 58.03; H, 4.17; N, 14.50, Found: C, 58.0; H, 4.17; N, 14.52.

FIGURE 14 Comparison of the cytotoxicity of the complex and the ligand with cisplatin measured with HCT116 and MCF-7 cell lines for 24, 48, and 72 h incubation

IR (KBr pellet, cm_1): ν (N-H) = 3309, ν (N-H) hydrazinic = 3138, ν (C=N) = 1597, ν (C=S) = 815. $_1$H NMR (400 MHz, DMSO-d_6) δ 11.86 (s, 1H, NH, H4), 10.16 (s, 1H, NH, H5), 8.15 (s, 1H, N=CH, H6), 7.96 (d, J = 8.4, 2H, CH-CH-CCl, H8), 7.57 (d, J = 7.2, 2H, CH-CH-CNH, H3), 7.49 (d, J = 8.4, 2H, CH-CH-CCl, H7), 7.38 (t, J = 7.2, 2H, CH-CH-CNH, H2), 7.23 (t, J = 7.2, 1H, CHCH-CH, H1). $_{13}$C NMR (101 MHz, DMSO-d_6) δ 176.7 (s, C5), 141.9 (s, C6), 139.5 (s, C_{IV}), 134.9 (s, C_{IV}), 133.5 (s, C_{IV}), 129.7 (s, C9), 129.2 (s, C8), 128.5 (s, C2), 126.4 (s, C3), 125.9 (s, C1).

4.3 | Synthesis of [pd(4-ClC$_6$H$_4$CHN=NC(S)NHPh)]$_4$ (compound 2)

To a solution of 100-mg potassium tetrachloropalladate (0.30 mmol) in 5 ml deionized water, 50-ml ethanol was added. The obtained fine yellow suspension of potassium tetrachloropalladate was treated with the 97-mg ligand (0.33 mmol). The reaction was proceeded at 40C for 4 days. The orange-yellowish product was isolated by vacuum filtration, washed with ethanol (40 ml) and dried at oven at 50C. The resulting ligand was isolated and characterized as follows: orange-yellow solid (75%); mp: 315–318C (dec.). Anal. calcd for $C_{56}H_{40}Cl_4N_{12}S_4Cl_4Pd_4$: C,

42.66; H, 2.56; N, 10.66, Found: C, 42.71; H, 2.53; N,
10.68. IR (KBr pellet, cm_1): ν (N-H) = 3309, ν (N-H)
$_{hydrazinic}$ = 3138, ν (C=N) = 1597, ν (C=S) = 815. $_1$H NMR (300 MHz, DMSO-d_6) δ 9.61 (s, 0.4H, NH), 9.34 (s,
0.6H, NH), 8.13 (d, J = 8.7 Hz, 0.4H), 8.06 (d, J = 8.7 Hz,
0.6H), 7.75 (d, J = 7.8 Hz, 1H), 7.54–7.42 (m, 2H), 7.35–
7.28 (appt, J = 8.2 Hz, 2H), 7.12 (dd, J = 8.0, 2.1 Hz, 1H),
7.04 (t, J = 7.4 Hz, 1H), 6.96 (d, J = 2.4 Hz, 1H). $_{13}$C NMR (75 MHz, DMSO-d_6) δ 168.1 (s, C_{IV}), 162.9 (s, C_{IV}),
162.8 (s, CH7), 147.2 (s, C_{IV}), 141.3 (s, C_{IV}), 133.5 (s,
$CH3_0$), 133.1 (s, C_{IV}), 129.1 (s, CH2), 129.0 (s, $CH2_0$),
128.9 (s, CH6), 124.4 (s, CH8), 123.4 (s, CH1), 121.1 (s,
CH3), 120.8 (s, CH9). HRMS (ESI) detection of signals
m/z = 1574.715 ± 0.007; m/z calcd for [$C_{56}H_{39}N_{12}S_4Cl_4Pd_4$]: 1574.7215.

4.4 | Culture medium and cell lines

The colorectal carcinoma cell line and the MCF7 human
breast adenocarcinoma cell line were supplied by the
National Cell Bank of Pasteur Institute, Tehran, Iran.
The cells were cultured in Dulbecco's Modified Eagle
Medium (DMEM) supplemented with 10% heatinactivated fetal bovine serum (FBS), 100 Uml_1 penicillin, 100 μgml_1 streptomycin, and 5-mM L-glutamine.
The cell lines were subsequently cultured at 37C in a
humidified atmosphere containing 5% CO_2. All reagents
and cell culture medium were provided by Gibco (Germany).

4.5 | Cytotoxicity assay

MTT [3-(4,5-dimethylthiazol-2-yl)-2,5-diphenyltetrazolium bromide] was used to evaluate the cytotoxic
activity of the complex. The test is based on the soluble
MTT metabolic reduction by mitochondrial enzyme
activity of viable tumor cells to produce an insoluble colored formazan that can be spectrophotometrically measured by dissolution in dimethyl sulfoxide (DMSO).
Cytotoxicity assay was performed by seeding 200 µl of the
cell suspension (5 10_4 $cellsml_1$) in 96-well plates and
incubated for 24 h (37C, 5% CO_2 humidified air). Afterwards, 20 µl of the prepared solutions of each compound
was added to each well. The compounds were dissolved
in DMSO prior to adding to the culture medium. The
control and treatment groups contained identical DMSO
concentrations of 0.5% (v/v). For evaluation of cytotoxicity, 20 µl of the MTT solution (5 $mgml_1$ in phosphate
buffer saline) was added in 48 h into the incubation and
the plates were incubated for another 3 h. Subsequently,
150 µl of the medium containing MTT was slowly
substituted with DMSO and pipetted to dissolve any
formazan crystal formed. Absorbance values at 560 nm
were determined using an ELISA plate reader (Awareness Technology, Stat Fax 2100).

4.6 | Molecular docking

The geometry optimization was separately performed for
the ligand structure and for the complex structure at first,
prior to docking calculations. Gaussian 09 Quantum
Chemistry package[86] was used for the optimization procedures and semiempirical methods employing PM6
functional[87] were carried out for them. The structure of
DNA with the PDB ID: 4QLC was obtained from the
Protein Data Bank (PDB). The resolution of chosen DNA
was 3.5 Å. As it is explained, the complex has the antimalaria effect so the authors believe that it is interesting
to investigate the interaction of the complex with the coronaviruses theoretically. So the structures of human coronavirus Mers and coronavirus disease 2019 with the PDB
ID 5ZVK and 6YB7 were obtained from PDB at

the resolutions of 3.31 Å and 1.25 Å, respectively. It should be noticed that it was not possible for the authors to investigate these interactions experimentally. The Autodock 4.2 software[88] was employed to perform the molecular docking calculations. The Lamarckian genetic algorithm(LGA)[89] was used during the calculations. In order to prepare the input file of DNA all the hetero atoms and the water molecules were removed primarily. The protein molecules were processed by adding all hydrogen, merging non-polar hydrogen atoms using AutoDock Tools.
The charges were assigned using the Gasteiger method.
The standard values were used for docking parameters.
Before the docking without any prior knowledge of the target pocket, the blind docking is needed. To find a favorable protein-ligand complex pose the whole surface of the receptor (DNA, human coronavirus Mers and coronavirus disease 2019) is scanned and the possible binding sites and the highest binding affinity is identified.[90,91] After the blind docking, the focus docking was done. In the process of docking, the size of the grid map were set to 126 126 126 $Å^3$ for DNA and 90 90 90 $Å^3$ and 90 90 90 $Å^3$ for the human coronavirus Mers and coronavirus disease 2019, respectively. A grid-point spacing of 0.375 Å that is roughly a quarter of the length of a carbon–carbon single bond was used in the AutoGrid runs. The conformations were ranked according to the lowest free binding energy. It is noteworthy that the structures were considered as flexible cases during docking.

ACKNOWLEDGMENTS
This study was supported by Iran Polymer and Petrochemical Institute and the Iran National Science Foundation under contract number 97006605.

AUTHOR CONTRIBUTIONS
Hossein Ali Khonakdar: Conceptualization. Ali Akbari: Data curation; investigation; project administration. Maryam Dehdashti Jahromi: Software. Azar Ramezanpour: Visualization. Anthony Kermagoret: Data curation; supervision. Abolfazl Heydari: Data curation; methodology. Esmaiel Jabbari: Investigation.

DATA AVAILABILITY STATEMENT
Data are openly available in a public repository that issues datasets with DOIs.

REFERENCES
[1] S. Schoch, L. K. Batchelor, T. Funaioli, G. Ciancaleoni, S. Zacchini, S. Braccini, F. Chiellini, T. Biver, G. Pampaloni, P. J. Dyson, Organometallics. 2020, 39, 361.
[2] A. Velasquez, R. A. de Souza, T. G. Passalacqua, A. R. Ribeiro, M. Scontri, C. M. Chin, L. de Almeida, M. L. Del Cistia, J. A. da Rosa, A. E. Mauro, J. Braz. Chem. Soc. 2016, 27, 1032.
[3] G. Jaouen, A. Vessieres, I. S. Butler, Acc. Chem. Res. 1993, 26, 361.
[4] J. Dupont, C. S. Consorti, J. Spencer, Chem. Rev. 2005, 105, 2527.
[5] S. Sangeetha, M. Murali, Int. J. Biol. Macromol. 2018, 107, 2501.
[6] E. G. Rodrigues, L. S. Silva, D. M. Fausto, M. S. Hayashi, S. Dreher, E. L. Santos, J. B. Pesquero, L. R. Travassos, A. C. F. Caires, Int. J. Cancer 2003, 107, 498.
[7] A. C. F. Caires, E. T. Almeida, A. E. Mauro, J. P. Hemerly, S. R. Valentini, Quim. Nova 1999, 22, 329.
[8] J. D. Higgins III, L. Neely, S. Fricker, J. Matthey, J. Inorg. Biochem. 1993, 49, 149.
[9] G. A. da Cunha, R. F. F. de Souza, R. L. de Farias, M. B. Moreira, D. E. S. Silva, R. D. Zanetti, D. M. Garcia, D. G. Spindola, L. F. G. Michelin, C. Bincoletto, J. Inorg. Biochem. 2020, 203, 110944.
[10] V. W. R. Moraes, A. C. F. Caires, E. J. Paredes-Gamero, T. Rodrigues, Cell Death Dis. 2013, 4, e658.
[11] D. P. Santana, P. A. Faria, E. J. Paredes-Gamero, A. C. F. Caires, I. L. Nantes, T. Rodrigues, Biochem. J. 2009, 417, 247.
[12] M. Carreira, R. Calvo-Sanjuan, M. Sanaú, I. Marzo, M. Contel, Organometallics 2012, 31, 5772.
[13] J. Albert, S. García, J. Granell, A. Llorca, M. V. Lovelle, V. Moreno, A. Presa, L. Rodríguez, J. Quirante, C. Calvis, J. Organomet. Chem. 2013, 724, 289.

[14] A. G. Quiroga, J. M. Pérez, I. Lopez-Solera, J. R. Masaguer, A.
Luque, P. Roman, A. Edwards, C. Alonso, C. NavarroRanninger, J. Med. Chem. 1998, 41, 1399.
[15] E. J. Siddiqui, I. Azad, A. R. Khan, T. Khan, J. Drug Deliv.
Ther. 2019, 9, 689.
[16] P. Genova, T. Varadinova, A. I. Matesanz, D. Marinova, P.
Souza, Toxicol. Appl. Pharmacol. 2004, 197, 107.
[17] S. A. Khan, M. Yusuf, Eur. J. Med. Chem. 2009, 44, 2270.
[18] C. Gan, J. Cui, S. Su, Q. Lin, L. Jia, L. Fan, Y. Huang, Steroids
2014, 87, 99.
[19] N. P. Prajapati, H. D. Patel, Synth. Commun. 2019, 49, 2767.
[20] D. L. Klayman, J. F. Bartosevich, T. S. Griffin, C. J. Mason,
J. P. Scovill, J. Med. Chem. 1979, 22, 855.
[21] A. K. Bhat, R. P. Bhamaria, R. A. Bellare, C. V. Deliwala,
Indian J. Chem. 1967, 5, 397.
[22] R. B. de Oliveira, E. M. de Souza-Fagundes, R. P. P. Soares,
A. A. Andrade, A. U. Krettli, C. L. Zani, Eur. J. Med. Chem.
2008, 43, 1983.
[23] D. C. Greenbaum, Z. Mackey, E. Hansell, P. Doyle, J. Gut,
C. R. Caffrey, J. Lehrman, P. J. Rosenthal, J. H. McKerrow, K.
Chibale, J. Med. Chem. 2004, 47, 3212.
[24] P. Chellan, N. Shunmoogam-Gounden, D. T. Hendricks, J.
Gut, P. J. Rosenthal, C. Lategan, P. J. Smith, K. Chibale, G. S.
Smith, Eur. J. Inorg. Chem. 2010, 2010, 3520.
[25] L. N. Suvarapu, A. V. Reddy, G. S. Kumar, S. O. Baek, J. Chem.
2011, 8, 1848.
[26] D. S. Kalinowski, P. Quach, D. R. Richardson, Future Med.
Chem. 2009, 1, 1143.
[27] L. E. Sarto, W. P. D. Badaro, E. P. de Gois, M. I. F. Barbosa, C.
Torres, R. B. Viana, J. Honorato, E. E. Castellano, E. T. de
Almeida, J. Mol. Struct. 2020, 1204, 127549.
[28] N. Cutillas, G. S. Yellol, C. de Haro, C. Vicente, V. Rodríguez,
J. Ruiz, Coord. Chem. Rev. 2013, 257, 2784.
[29] D. Kovala-Demertzi, A. Domopoulou, M. A. Demertzis, A.
Papageorgiou, D. X. West, Polyhedron 1997, 16, 3625.
[30] A. G. Quiroga, J. M. Pérez, I. Lopez-Solera, E. I. Montero, J. R.
Masaguer, C. Alonso, C. Navarro-Ranninger, J. Inorg. Biochem.
1998, 69, 275.
[31] A. G. Quiroga, J. M. Pérez, E. I. Montero, J. R. Masaguer, C.
Alonso, C. Navarro-Ranninger, J. Inorg. Biochem. 1998, 70, 117.
[32] M. Mohamadi, A. Hassankhani, S. Y. Ebrahimipour, M.
Torkzadeh-Mahani, Int. J. Biol. Macromol. 2017, 94, 85.
[33] R. Palchaudhuri, P. J. Hergenrother, Curr. Opin. Biotechnol.
2007, 18, 497.
[34] A. Soni, P. Khurana, T. Singh, B. Jayaram, Bioinformatics
2017, 33, 1488.
[35] V. Raj, J. G. Park, K.-H. Cho, P. Choi, T. Kim, J. Ham, J. Lee,
Int. J. Biol. Macromol. 2021, 168, 474.
[36] I. M. Ibrahim, D. H. Abdelmalek, A. A. Elfiky, Life Sci. 2019,
226, 156.
[37] A. A. Elfiky, S. M. Mahdy, W. M. Elshemey, J. Med. Virol.
2017, 89, 1040.
[38] L. Zhang, R. Zhou, J. Phys. Chem. B 2020, 124, 6955.
[39] T. R. Bal, B. Anand, P. Yogeeswari, D. Sriram, Bioorg. Med.
Chem. Lett. 2005, 15, 4451.
[40] V. Mishra, S. N. Pandeya, C. Pannecouque, M. Witvrouw, E.
De Clercq, Arch. Pharm. An Int. J. Pharm. Med. Chem. 2002,
335, 183.
[41] S. Adsule, V. Barve, D. Chen, F. Ahmed, Q. P. Dou, S. Padhye,
F. H. Sarkar, J. Med. Chem. 2006, 49, 7242.
[42] K. Karami, Z. Mehri Lighvan, H. Farrokhpour, M. Dehdashti
Jahromi, A. A. Momtazi-borojeni, J. Biomol. Struct. Dyn. 2018,
36, 3324.
[43] K. Karami, Z. M. Lighvan, S. A. Barzani, A. Y. Faal, M.
Poshteh-Shirani, T. Khayamian, V. Eigner, M. Dušek, New
J. Chem. 2015, 39, 8708.
[44] Z. M. Lighvan, H. A. Khonakdar, A. Heydari, M. Rafiee, M. D.
Jahromi, A. Derakhshani, A. A. Momtazi-Borojeni, Appl. Organomet. Chem. 2020, 34, e5839.
[45] K. Karami, M. Rafiee, Z. M. Lighvan, M. Zakariazadeh, A. Y.
Faal, S.-A. Esmaeili, A. A. Momtazi-Borojeni, J. Mol. Struct.
2018, 1154, 480.
[46] K. Karami, Z. M. Lighvan, A. M. Alizadeh, M. PoshtehShirani, T. Khayamian, J. Lipkowski, RSC Adv. 2016, 6, 78424.
[47] K. Karami, Z. M. Lighvan, M. D. Jahromi, J. Lipkowski, A. A.
Momtazi-borojeni, J. Organomet. Chem. 2017, 827, 1.
[48] J. Martínez, M. T. Pereira, J. M. Ortigueira, B. Bermúdez, J. M.
Antelo, A. Fernandez, J. M. Vila, Polyhedron 2012, 31, 217.
[49] J. M. Antelo, L. Adrio, M. T. Pereira, J. M. Ortigueira, J. J.
Fernandez, J. M. Vila, Cryst. Growth Des. 2010, 10, 700.
[50] D. X. West, J. S. Ives, G. A. Bain, A. E. Liberta, J. ValdésMartínez, K. H. Ebert, S. Hernandez-Ortega, Polyhedron 1997,
16, 1895.

[51] H. Onoue, I. Moritani, J. Organomet. Chem. 1972, 43, 431.
[52] A. A. Ali, H. Nimir, C. Aktas, V. Huch, U. Rauch, K.-H.
Schäfer, M. Veith, Organometallics 2012, 31, 2256.
[53] A. G. Quiroga, C. N. Ranninger, Coord. Chem. Rev. 2004,
248, 119.
[54] P. Chellan, S. Nasser, L. Vivas, K. Chibale, G. S. Smith,
J. Organomet. Chem. 2010, 695, 2225.
[55] E. Ramachandran, D. Senthil Raja, N. P. Rath, K. Natarajan,
Inorg. Chem. 2013, 52, 1504.
[56] L.-R. Lin, Q.-J. Xu, X. Wu, R.-B. Huang, L. Zheng, J. Fluoresc.
2011, 21, 1319.
[57] K. Karami, A. Ramezanpour, M. Zakariazadeh, A. Shahpiri,
M. Kharaziha, A. Kazeminasab, ChemistrySelect 2019, 4, 5126.
[58] N. Shahabadi, N. H. Moghadam, Spectrochim. Acta Part A
Mol. Biomol. Spectrosc. 2012, 96, 723.
[59] P. J. Cox, G. Psomas, C. A. Bolos, Bioorg. Med. Chem. 2009, 17,
6054.
[60] A. Wolfe, G. H. Shimer Jr., T. Meehan, Biochemistry 1987, 26,
6392.
[61] L. M. M. Vieira, M. V. de Almeida, M. C. S. Lourenço, F. A.
F. M. Bezerra, A. P. S. Fontes, Eur. J. Med. Chem. 2009, 44,
4107.
[62] H. M. Refaat, D. A. N. El-Din, J. Mol. Struct. 2018, 1163, 103.
[63] C.-C. Ju, A.-G. Zhang, C.-L. Yuan, X.-L. Zhao, K.-Z. Wang,
J. Inorg. Biochem. 2011, 105, 435.
[64] N. Shahabadi, F. Shiri, S. Hadidi, K. Farshadfar, S. Sajadimajd,
S. M. Roe, Spectrochim. Acta Part A Mol. Biomol. Spectrosc.
2020, 235, 118280.
[65] K. Cheung-Ong, G. Giaever, C. Nislow, Chem. Biol. 2013,
20, 648.
[66] L. H. Hurley, Nat. Rev. Cancer 2002, 2, 188.
[67] J. Andersson, M. Li, P. Lincoln, Chem. A Eur. J. 2010, 16,
11037.
[68] T. Paramanathan, F. Westerlund, M. J. McCauley, I. Rouzina,
P. Lincoln, M. C. Williams, J. Am. Chem. Soc. 2008, 130, 3752.
[69] N. Shahabadi, S. Kashanian, M. Purfoulad, Spectrochim. Acta
Part A Mol. Biomol. Spectrosc. 2009, 72, 757.
[70] M. Hossain, G. S. Kumar, Mol. Biosyst. 2009, 5, 1311.
[71] T. Šmidlehner, I. Piantanida, G. Pescitelli, Beilstein J. Org.
Chem. 2018, 14, 84.
[72] M. Dustkami, H. Mansouri-Torshizi, Int. J. Biol. Macromol.
2017, 99, 319.
[73] J. Kypr, M. Vorlíc̆kova, Biopolym. Orig. Res. Biomol. 2002,
67, 275.
[74] N. Lohani, H. N. Singh, R. R. Moganty, Int. J. Biol. Macromol.
2016, 87, 433.
[75] Y.-M. Chang, C. K.-M. Chen, M.-H. Hou, Int. J. Mol. Sci. 2012,
13, 3394.
[76] Y.-S. Lo, W.-H. Tseng, C.-Y. Chuang, M.-H. Hou, Nucleic Acids
Res. 2013, 41, 4284.
[77] J. Andersson, P. Lincoln, J. Phys. Chem. B. 2011, 115, 14768.
[78] C. Bourdouxhe-Housiaux, P. Colson, C. Houssier, M. J.
Waring, C. Bailly, Biochemistry 1996, 35, 4251.
[79] C. Icsel, V. T. Yilmaz, M. Aygun, E. Ulukaya, Bioorg. Med.
Chem. Lett. 2020, 30, 127077.
[80] C. W. Mosher, K. F. Kuhlmann, D. G. Kleid, D. W. Henry,
J. Med. Chem. 1977, 20, 1055.
[81] S. Parveen, F. Arjmand, Q. Zhang, M. Ahmad, A. Khan, L.
Toupet, J. Biomol. Struct. Dyn. 2020, 1.
[82] M. Cory, D. D. McKee, J. Kagan, D. W. Henry, J. A. Miller,
J. Am. Chem. Soc. 1985, 107, 2528.
[83] P. Liu, J. Liu, Y.-Q. Zhang, B.-Y. Wu, K.-Z. Wang,
J. Photochem. Photobiol. B Biol. 2015, 143, 89.
[84] S. Perez, I. Tvaroška, Advances in carbohydrate chemistry and
biochemistry, Vol. 71, Elsevier 2014 9.
[85] F. Lopez-Vallejo, T. Caulfield, K. Martínez-Mayorga, M. A.
Giulianotti, A. Nefzi, R. A. Houghten, J. L. Medina-Franco,
Comb. Chem. High Throughput Screen. 2011, 14, 475.
[86] M. J. Frisch, G. W. Trucks, H. B. Schlegel, G. E. Scuseria,
M. A. Robb, J. R. Cheeseman, J. A. Montgomery, T. Vreven
Jr., K. N. Kudin, J. C. Burant, J. Comput. Chem. 2008, 29, 839.
[87] Y. Zhao, D. G. Truhlar, J. Chem. Phys. 2006, 125, 194101.
[88] G. M. Morris, R. Huey, W. Lindstrom, M. F. Sanner, R. K. Belew,
D. S. Goodsell, A. J. Olson, J. Comput. Chem. 2009, 30, 2785.
[89] G. M. Morris, D. S. Goodsell, R. S. Halliday, R. Huey, W. E.
Hart, R. K. Belew, A. J. Olson, J. Comput. Chem. 1998, 19, 1639.
[90] C. Hetényi, D. van der Spoel, FEBS Lett. 2006, 580, 1447.
[91] C. Hetényi, D. van der Spoel, Protein Sci. 2002, 11, 1729.

SUPPORTING INFORMATION

Additional supporting information may be found in the online version of the article at the publisher's website.

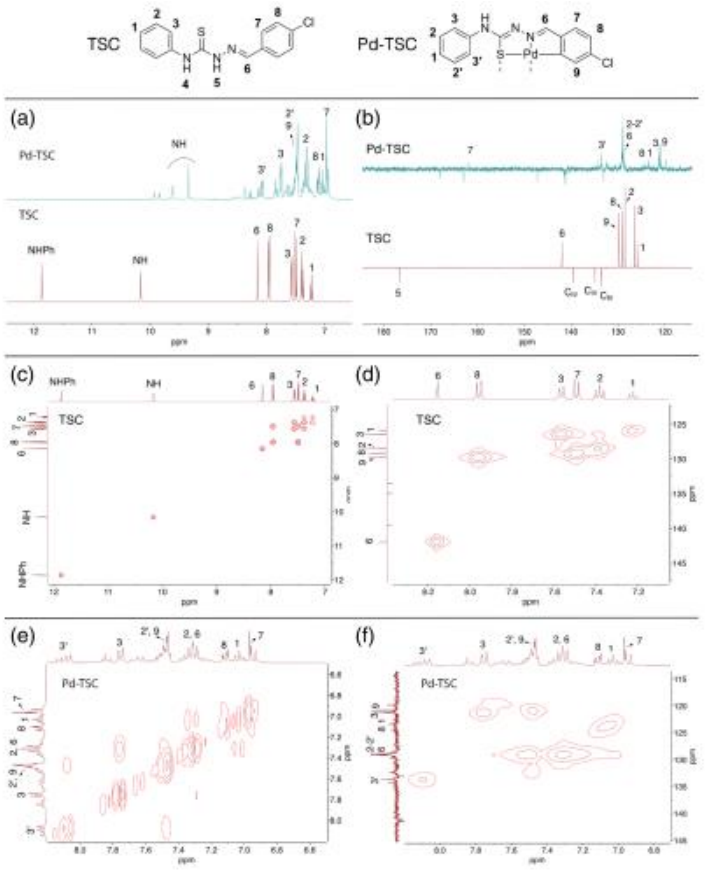

F I G U R E 1 (a) H-NMR Pd-TSC and TSC, (b) APT $_{13}$C NMR Pd-TSC and TSC, (c) TSC COSY, (d) TSC HMQC, (e) Pd-TSC COSY, and (f) Pd-TSC HMQC experiments

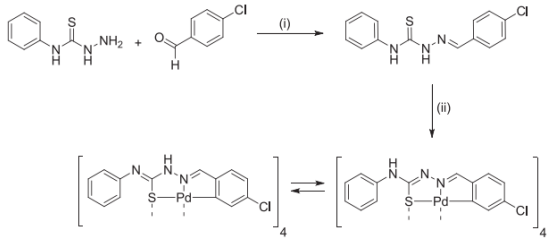

S C H E M E 1 Synthesis of thiosemicarbazone ligand and tetranuclear cyclopalladated complex. Reaction conditions: (i) MeOH, 25C, 18 h; (ii) $K_2[PtCl_4]$, EtOHH_2O, 40C, 4 days

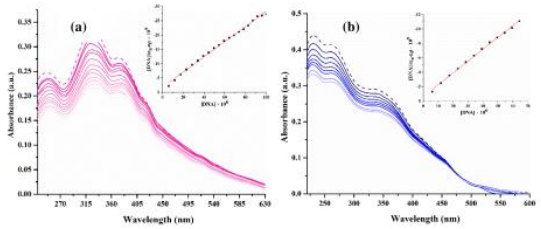

F I G U R E 2 Electronic spectra of (a) ligand and (b) palladium complex in buffer solution of 5-mM Tris–HCl/50 mM NaCl at pH = 7.2 following addition of the DNA. [Pd Complex] = 6 10_5 M, [DNA] = 0–6.5 10_5 M. Arrow shows the decrease in absorption intensity

upon increasing DNA concentration (Inset: plot of [DNAε_a ε_f] vs. [DNA] for determination of K_b)

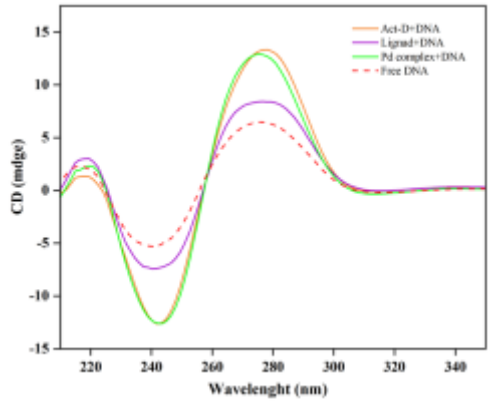

F I G U R E 4 CD spectrum of DNA (15 10_4 M) in 5-mM Tris–
HCl buffer with 50-mM NaCl (pH = 7.3) in the presence of ligand,
Pd complex, and ActD (7.5 10_5 M

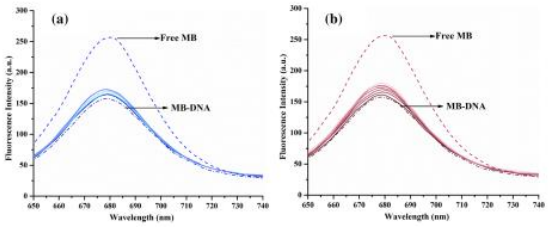

F I G U R E 3 The emission spectra of the DNA–MB, in the presence of (a) ligand and (b) palladium complex. [DNA] = 6 10_5 M, [MB] = 6 10_6 M, [Ligand] = [Pd complex] = 0–8 10_5. The arrow shows the change in emission intensity upon increasing concentration of the compounds

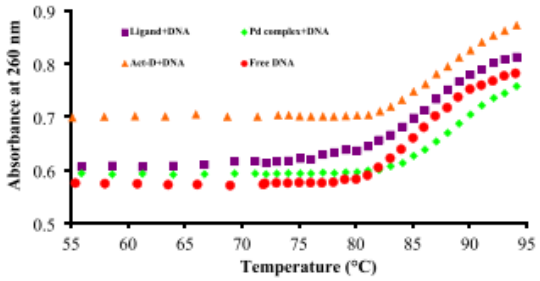

F I G U R E 5 The effect of heating on the absorbance of CT-DNA at 260 nm (7.5 10_6 M) in the absence and presence of ligand, Pd complex, and Act D (3.75 10_6 M) in 5-mM Tris–HCl with 50-mM NaCl

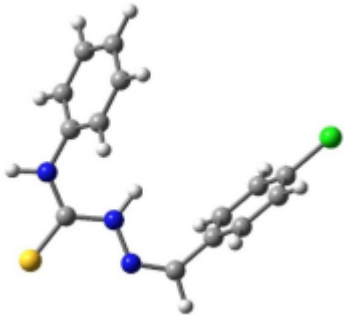

F I G U R E 6 The structure of the ligand optimized at semiempirical methods applying PM6

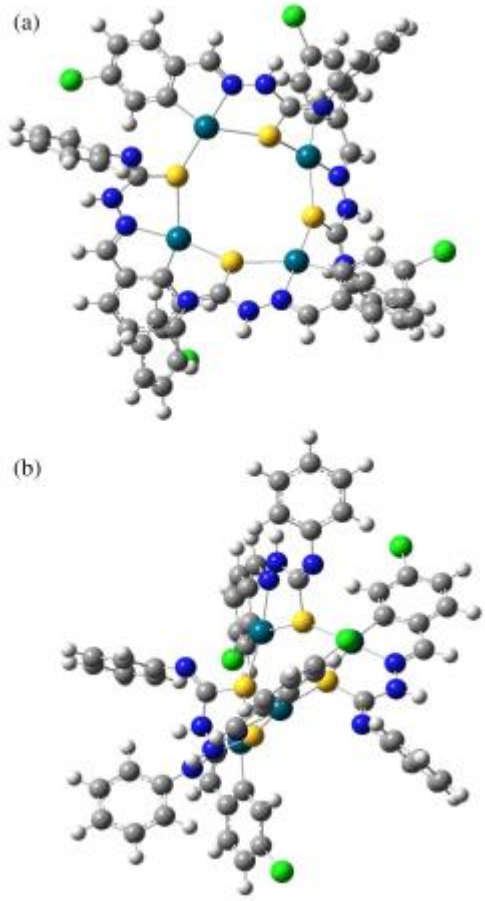

F I G U R E 7 The structure of the complex optimized at semiempirical methods applying PM6 from two points of view
(a and b)

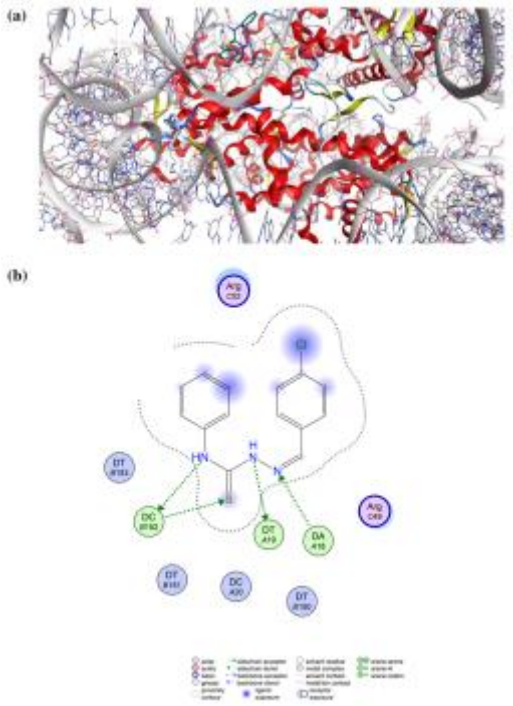

FIGURE 8 Results of docking procedure. (a) Predicted orientations of the lowest docking energy conformations of ligand with the threading intercalation of DNA. (b) Twodimensional interactions between ligand and DNA

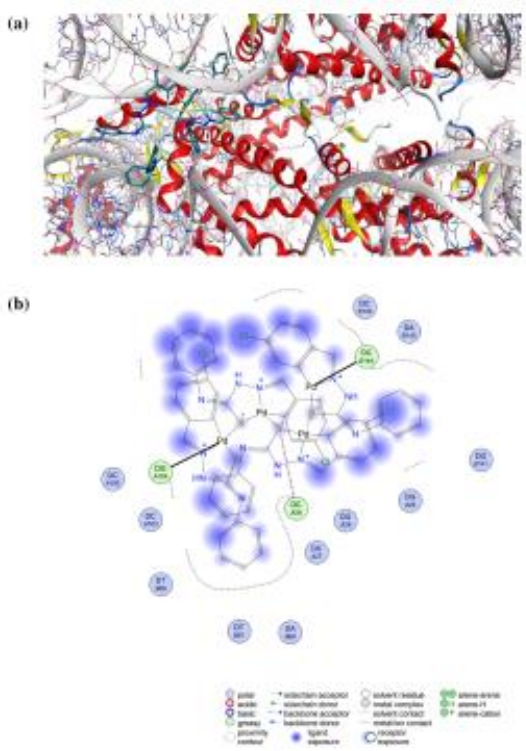

FIGURE 9 Results of docking procedure. (a) Predicted orientations of the lowest docking energy conformations of complex with the threading intercalation of DNA. (b) Twodimensional interactions between complex and DNA

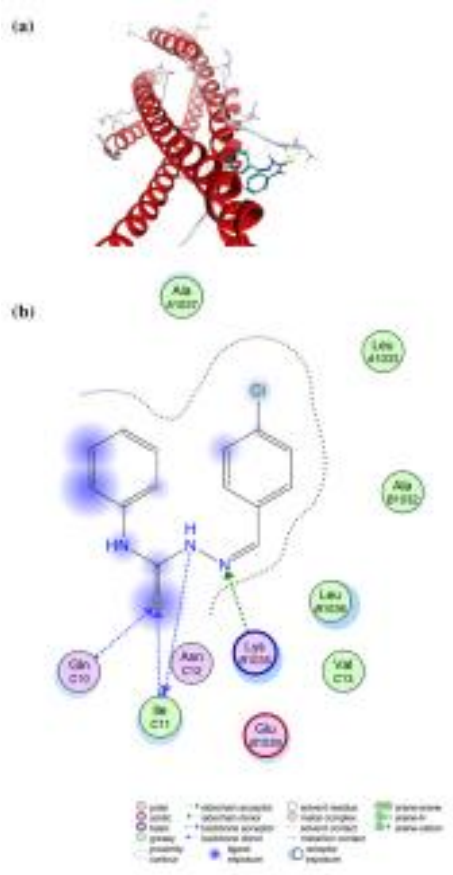

F I G U R E 1 0 Results of docking procedure. (a) Predicted orientations of the lowest docking energy conformations of ligand with the human coronavirus Mers. (b) Two-dimensional interactions between ligand with the human coronavirus Mers

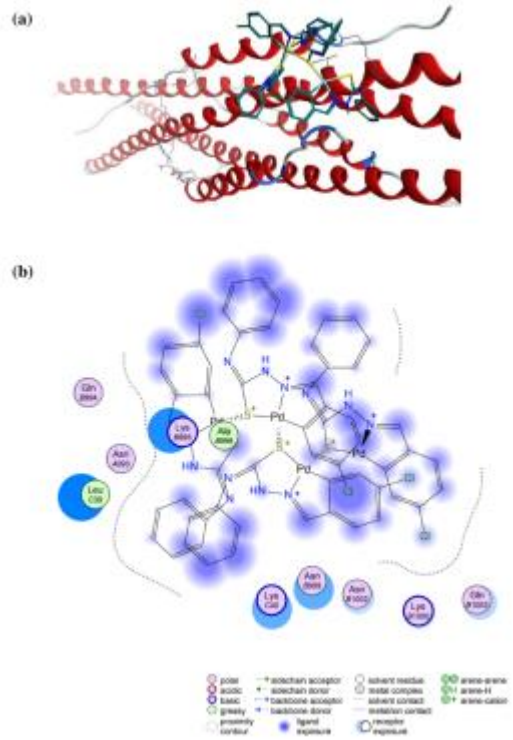

F I G U R E 1 1 Results of docking procedure. (a) Predicted orientations of the lowest docking energy conformations of complex with the human coronavirus Mers. (b) Twodimensional interactions between complex and the human coronavirus Mers

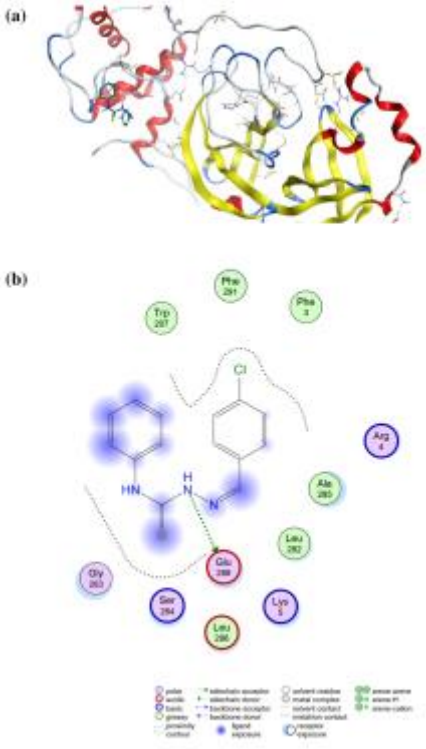

FIGURE 12 Results of docking procedure. (a) Predicted orientations of the lowest docking energy conformations of ligand with the coronavirus disease 2019. (b) Two-dimensional interactions between ligand and coronavirus disease 2019

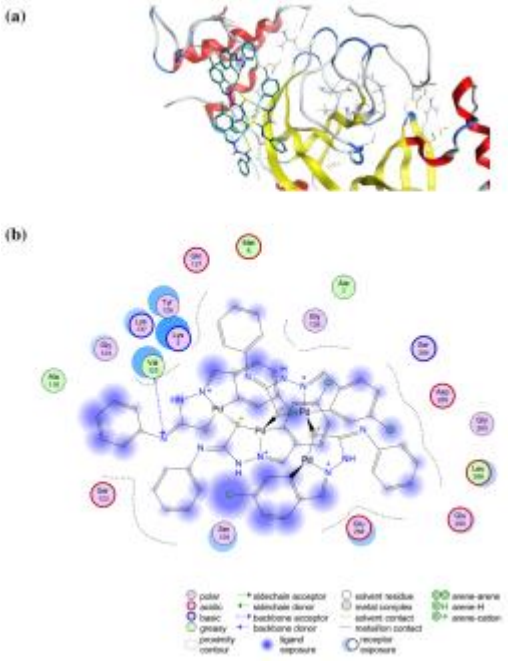

FIGURE 13 Results of docking procedure. (a) Predicted orientations of the lowest docking energy conformations of complex with the coronavirus disease 2019. (b) Twodimensional interactions between the complex and coronavirus disease 2019

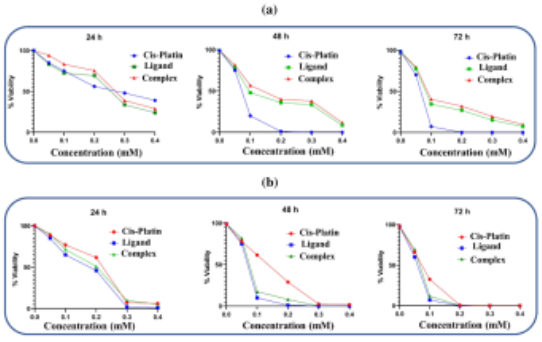

FIGURE 14 Comparison of the cytotoxicity of the complex and the ligand with cisplatin measured with HCT116 and MCF-7 cell lines for 24, 48, and 72 h incubation